RESEARCH ARTICLE

DUSE WILEY

Fluid-rock interaction experiments with andesite at 100°C for potential carbon storage in geothermal reservoirs

Grace E. Belshaw[1,2] | Elisabeth Steer[3] | Yukun Ji[1,2,4] | Herwin Azis[5] |
Benyamin Sapiie[6] | Bagus Muljadi[2,7] | Veerle Vandeginste[1,2,8] [ID]

[1]School of Chemistry, University of Nottingham, Nottingham, UK

[2]GeoEnergy Research Centre, University of Nottingham, Nottingham, UK

[3]British Geological Survey, Keyworth, UK

[4]State Key Laboratory of Intelligent Construction and Healthy Operation and Maintenance of Deep Underground Engineering, China University of Mining and Technology, Xuzhou, China

[5]PT Supreme Energy, Jakarta, Indonesia

[6]Faculty of Earth Sciences and Technology, Institut Teknologi Bandung, Bandung, Indonesia

[7]Faculty of Engineering, University of Nottingham, Nottingham, UK

[8]Department of Materials Engineering, KU Leuven, Campus Bruges, Bruges, Belgium

Correspondence
Veerle Vandeginste
Email: veerle.vandeginste@kuleuven.be

Funding information
Engineering and Physical Sciences Research Council, Grant/Award Number: EP/M000567/1

Abstract
Geothermal energy extraction often results in the release of naturally occurring carbon dioxide (CO_2) as a byproduct. Research on carbon storage using volcanic rock types other than basalt under both acidic and elevated temperature conditions has been limited so far. Our study uses batch reactor experiments at 100°C to investigate the dissolution of andesite rock samples obtained from an active geothermal reservoir in Sumatra (Indonesia). The samples are subjected to reactions with neutral-pH fluids and acidic fluids, mimicking the geochemical responses upon reinjection of geothermal fluids, either without or with dissolved acidic gases, respectively. Chemical elemental analysis reveals the release of Ca^{2+} ions into the fluids through the dissolution of feldspar. The overall dissolution rate of the rock samples is 2.4×10^{-11} mol/(m$^2 \cdot$ s) to 4.2×10^{-11} mol/(m$^2 \cdot$ s), based on the Si release during the initial 7 h of the experiment. The dissolution rates are about two orders of magnitude lower than those reported for basaltic rocks under similar reaction conditions. This study offers valuable insights into the potential utilization of andesite reservoirs for effective CO_2 storage via mineralization.

KEYWORDS
andesite, carbon sequestration, geothermal reservoirs, plagioclase dissolution

Highlights
- Geothermal energy production can release naturally occurring carbon dioxide.
- Calcic plagioclase-rich andesite samples release increased divalent ions.
- Higher plagioclase content in samples correlates with elevated buffering capacity.
- Occurrence of secondary Al-containing mineral formation is likely.
- Andesite dissolution rate is 10–100 times slower than that of basalt.

1 | INTRODUCTION

A steady increase in carbon dioxide (CO_2) emissions has been documented since the 1950s, primarily attributed to human activities, such as the burning of fossil fuels (Department of Energy and Climate Change, 2016; Edenhofer et al., 2014; McCarthy et al., 2001). To mitigate the potential global temperature increase beyond 1.5°C compared to preindustrial levels, it is imperative to transition from fossil fuels to renewable energy sources and implement technologies for capturing and storing excess CO_2 (Intergovernmental Panel on Climate Change [IPCC], 2018).

Geothermal energy, a renewable energy source, has been successfully harnessed for heat and electricity generation in various parts of the world. However, geothermal reservoirs, often located in volcanic regions, present a significant challenge due to the release of naturally occurring volcanic gases, including CO_2 and H_2S, during production (Fridriksson et al., 2016). Although CO_2 emissions from geothermal power plants are approximately 20 times lower than those from coal-burning plants of equivalent size, addressing all greenhouse gas emissions is essential to establish geothermal energy as a truly clean and renewable source (Aradóttir et al., 2015). In the case of Indonesia, which possesses an estimated 40% of the world's geothermal resources, a scientifically informed mitigation strategy could unlock the potential for vast carbon-neutral energy sources (Suharmanto et al., 2015).

In several field trials involving subsurface basaltic systems, the injection of CO_2 dissolved in aqueous fluids has proven successful in sequestering CO_2 through mineralization. Subsurface storage of CO_2 can involve several trapping mechanisms, such as structural, residual, solubility, and mineralization trapping. Structural trapping requires an impermeable layer overlying the reservoir to prevent escape of CO_2 gas back to the surface, whereas mineralization trapping can be considered a safer long-term storage mechanism. The CarbFix project in Iceland, at the Hellisheidi Geothermal Power Plant, demonstrated a remarkable 95% sequestration of the injected CO_2 in just 2 years (Clark et al., 2019; Gíslason et al., 2018; Matter et al., 2016; Pogge von Strandmann et al., 2019; Snæbjörnsdóttir et al., 2020). Results from CarbFix2, which doubled the CO_2 injection rate, showed the mineralization of 50%–60% of the injected CO_2 within 2 years, with no detectable change in host rock permeability (Clark et al., 2020). A transport model established for long-term CO_2 injection into these basaltic rocks at Hellisheidi aligns with field measurements and estimates a theoretical maximum storage capacity for the reservoir at 300 megatons of CO_2 by 2050, assuming a 10% filling of the available space (Ratouis et al., 2022). This study suggested that the precipitation of calcium carbonate could have been limited by the interaction between the fluids and basalt host rock, in particular, the release of calcium from the rock into the fluids. Another notable field demonstration is the Wallula Basalt Pilot test in the United States, which achieved the sequestration of injected supercritical CO_2 within 2 years of placement (McGrail et al., 2011, 2017). Furthermore, preinjection tests and geochemical modeling conducted on the Nesjavellir geothermal system in Iceland indicated that injected CO_2-charged fluids would dissolve the altered basaltic host rock near the injection well and subsequently trigger carbonate precipitation between the injection well and the production well (Galeczka et al., 2022). Basaltic rocks are favored for their high content of olivine, pyroxene, and plagioclase. Olivine and pyroxene have thermodynamically favorable dissolution rates under acidic CO_2 injection conditions, facilitating the release of alkaline earth metal cations that can lead to carbonate precipitation, as illustrated in the following equation (Gislason et al., 2010; Hangx and Spiers, 2009; Matter et al., 2007; McGrail et al., 2006).

$$(Ca, Mg, Fe)^{2+} + CO_2 + H_2O \leftrightarrow (Ca, Mg, Fe)CO_3 + 2H^+. \tag{1}$$
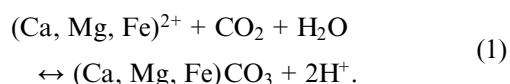
Equation (1) suggests that H^+ ions must be consumed to favor the formation of solid carbonates, enabling carbon sequestration. Mafic rocks, such as basalts, possess a high neutralization capacity, providing alkaline earth metal cations upon dissolution, which can further contribute to carbonate mineral formation (Matter et al., 2007).

Importantly, geothermal energy can be harnessed from a wider array of rock systems beyond basalt. For instance, Indonesia, rich in geothermal energy resources (Sawin et al., 2017), features reservoir systems composed of andesitic rocks (Boedihardi et al., 1993; Purnomo and Pichler, 2014). Andesite is found in various parts of the world, including Central and South America and multiple locations in Australasia. Nevertheless, research on carbon sequestration in rock types other than basalt remains relatively limited. A recent study on reactive transport modeling of the Kizildere geothermal field in Turkey indicated a prevalence of CO_2 solubility trapping and a lack of trapping through carbonate mineralization in metamorphic schist and marble host rocks at 220°C (Erol et al., 2023). The limited CO_2 mineralization in this case can be attributed to (i) the scarcity of divalent cations, such as Mg^{2+}, Ca^{2+}, and Fe^{2+}, in the chemical system and (ii) fluid-rock interaction that is primarily controlled by K–Al–Si-containing minerals, for example, muscovite. Batch reactor experiments with rhyolite rock and supercritical CO_2 at temperatures ranging from 150 to 170°C and pressures of 35 MPa led to the dissolution of primarily calcite and K-feldspar, and precipitation of calcite and ankerite (Na et al., 2015). Similarly, fractured granite rock samples were used in water–CO_2–rock interaction core flooding experiments in a study on CO_2-based enhanced geothermal systems at 200°C. The results indicated the predominant dissolution of feldspars and the precipitation of mainly calcite and dolomite (Wu et al., 2021). However, other experiments on CO_2-saturated granite geothermal systems at 250°C showed the dissolution of K-feldspar, oligoclase, and epidote, along with the precipitation of smectite (Lo Ré et al., 2014). Carbonate precipitation was only observed upon cooling and degassing, suggesting that longer time scales are necessary for its formation (Lo Ré et al., 2014). Certain studies reported on reactions between acidic fluids and various volcanic glass samples, primarily from Iceland (Wolff-Boenisch et al., 2004, 2006), which revealed a slower dissolution rate for glasses with higher silica content. Consequently, some expected trends could also be proposed regarding the dissolution behavior of rocks that have a less amorphous, more crystalline structure. The dissolution rates in these studies were used to determine calcium release rates, enabling interpretations and estimations of the CO_2 consumption capacity of the samples. Nevertheless, these studies primarily focused on ambient temperature and a pH value of 4 or higher, and the samples used were mainly volcanic glass or individual mineral samples, as opposed to rock samples containing crystalline minerals. A recent study presented geochemical modeling results for CO_2 injection in the Ungaran geothermal field in Java Island, Indonesia, using data on rock mineralogy and geothermal water chemistry (Utomo and Güleç, 2021). The latter study represented one of the first modeling efforts conducted on intermediate volcanic rock (andesite) geothermal reservoir, and indicated promising results for carbon trapping through mineralization. However, this study concentrated solely on modeling, and has yet to be validated by experimental data.

The primary objectives of this study are twofold: (i) to investigate the geochemical reactions occurring between andesitic rocks and representative geothermal reservoir fluids in Sumatra Island, Indonesia, and (ii) to assess the implications of these fluid–rock interactions

for potential implementation of carbon storage technology involving mineral formation through the reinjection of CO_2 dissolved in fluids into andesite geothermal reservoirs, in order to assist in determining whether this is a viable sequestration method if basaltic reservoirs are not available within the relevant geographic area.

This study is exclusively focused on andesitic rock types for potential carbon sequestration. Note that an assessment of the field-scale potential of carbon sequestration would also need to examine other factors, such as rock permeability, particularly of the overlying layers, to ensure that the system has some structural and residual carbon trapping potential as well.

2 | MATERIALS AND METHODS

2.1 | Rock samples

For our experiments, we utilized samples collected from a geothermal field located on Sumatra Island, Indonesia. The geological formation of Sumatra Island resulted from the subduction of the Sundaland Continental Plate beneath the India–Australia Oceanic Plate. The tectonic stress generated by this subduction process, known as the Subduction of Sundaland with India–Australia, gave rise to dextral strike–slip faults that run parallel to Sumatra Island, notably the Great Sumatra Fault (GSF). In addition to the GSF, this subduction activity also led to the formation of a volcanic arc, causing seismic events and creating geothermal potential in Sumatra Island (Muraoka et al., 2010; Santoso et al., 1995). As described by Sieh and Natawidjaja (2000), the GSF spans a length of 1900 km and comprises 19 segments of dilatational step-overs, each segment ranging from 60 to 200 km in length (Sieh and Natawidjaja, 2000).

The prevailing mineralogical composition in the region is primarily andesitic in nature (Barber et al., 2005), consistent with observations from drill cores obtained from the Quaternary-aged andesitic–basaltic volcanic rocks extending from the surface down to the top of the reservoir section. The reservoir section itself comprises Tertiary-aged mixed marine sediment interspersed with layers of silicic and andesitic volcanic rocks.

For our research, we received three rock core samples from the geothermal field in Sumatra, graciously provided by PT Supreme Energy. These samples, denoted as RDB1, RDC1, and RDI1, were extracted from exploration wells at depths ranging from approximately 1 to 2 km (Supreme Energy, 2019).

2.2 | Sample preparation and characterization

An overview of sample preparation, characterization, batch reactor experiments, and postexperimental analysis is presented schematically in Figure 1. To begin, each sample was crushed using an agate pestle and mortar. The clay fraction (particles ≤2 μm) of each sample was then determined using a specific aqueous dispersion and centrifugation method: A 5 g portion of each sample was suspended in a 50 mL solution comprising ultrapure MilliQ (MQ) water, 3% hydrogen peroxide (H_2O_2), and 4 g/L of sodium hexametaphosphate (SHMP). This mixture was placed in an ultrasonic bath for 2 h, serving to eliminate organic materials and disperse the clay. Subsequently, a sequence of centrifugation and washing steps at 4000 r/min for 30 min per cycle was performed until the liquids became clear. The solid samples were then resuspended in MQ water and subjected to sonication for 15 min to ensure that the clay remained evenly dispersed. Finally, a shorter centrifugation step lasting 2 min at 1000 r/min was carried out and the resulting clay suspension (comprising particles ≤2 μm in diameter) was carefully decanted to separate it.

To distinguish between chlorite and kaolinite clay peaks in the powder X-ray diffraction (PXRD) patterns, a hydrochloric acid (HCl) treatment was applied to each separated clay fraction (Biscaye, 1964). In a teflon vial, 0.4 mL of 12.4 M HCl was combined with 4.6 mL of the clay suspension. The vial was sealed and heated to 150°C for 1 h on a hotplate. Following this treatment, the sample was allowed to cool before washing by centrifugation.

Mineralogical phase identification through PXRD was conducted using an X'Pert PRO PANalytical MPD X-ray Diffractometer. Normal Bragg–Brentano geometry was used, with CuKα radiation at 40 kV and 40 mA, utilizing sample holders with a 20 mm diameter. Samples were scanned over a sampling range from 5° to 70° 2θ, with a step size of 0.0066 and a scan speed of 0.23° 2θ/s. Bulk powder samples were pressed into 20 mm holders for analysis. In the case of clay experiments, 700 μL of each clay suspension was pipetted onto 20 mm glass
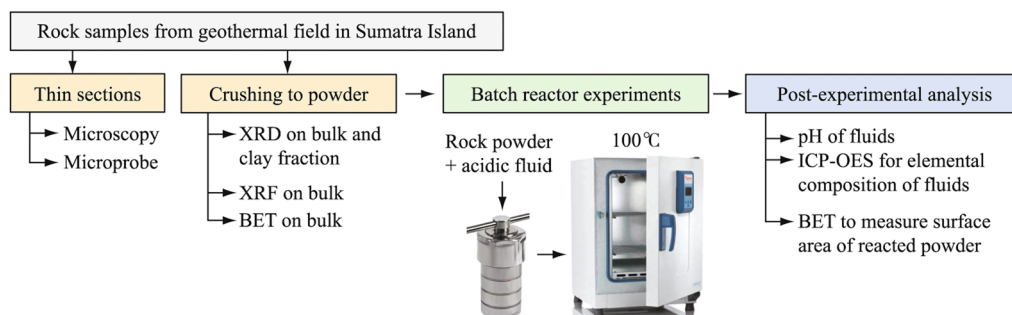

FIGURE 1 Schematic overview of the rock sample preparation, characterization, batch reactor experiments, and postexperimental analysis in this study. ICP-OES, inductively coupled plasma optical emission spectrometer; BET, Brunauer-Emmett-Teller.

discs, with the addition of two drops of acetone, and left to air-dry overnight before being placed in sample holders for analysis. For phase identification and semiquantitative analysis, the PDF4 database (International Centre for Diffraction Data [ICDD], 2018) was utilized within DIFFRAC.EVA software to identify mineral peak patterns.

The elemental composition of the powdered samples was analyzed using X-ray fluorescence (XRF) with an Epsilon 3 XL high performance benchtop energy-dispersive X-ray fluorescence spectrometer system.

Nitrogen Brunauer-Emmett-Teller (BET) analysis was conducted on a Micromeritics 3flex Surface Characterization Analyzer at 77 K, encompassing partial pressures ranging from 0 to 0.99, to determine the surface area of the samples. Before analysis, the powdered rock samples were degassed overnight at 100°C. The surface area was found to be $1.1 \pm 0.1 \, m^2/g$ for RDB1, $1.7 \pm 0.1 \, m^2/g$ for RDC1, and $1.8 \pm 0.1 \, m^2/g$ for RDI1 (error based on two replicates).

To gain textural and mineralogical insights into each sample, 30 μm thin sections were examined using a Carl Zeiss Axio Scope A1 optical microscope equipped with reflective and transmitted light modes and polarizing filters positioned above and below the sample stage. Images were captured using a Zeiss Axiocam ERc camera.

The chemical composition of the mineral phases in the thin sections was determined using standard wavelength-dispersive techniques with a JEOL JXA-8200 electron microprobe. This involved using a 15.0 kV, 20 nA electron beam at a working distance of 11 mm. Before analysis, the thin sections were coated with a 15 nm layer of carbon.

2.3 | Batch reactor experiments

In this study, we use batch reactor experiments to assess the reaction between andesite powder and neutral or acidic fluids at 100°C. The benefits of this method are the safe facile setup, the use of fine homogeneous rock powder with determined reactive surface area enabling good contact of each component of the rock with the fluid, and good reproducibility and quantification. Although the use of batch reactor experiments with powdered rock samples does not simulate the flow characteristics of the fluid in the pore structure of the rock, they do allow us to conduct multiple duplicated experiments to estimate the whole-rock sample dissolution rates. Core flooding-type or similar experiments would be needed to examine the effects of the flow characteristics within the rock samples, which would not provide the desired duplication ability for this particular study examining whole-rock dissolution rates to generate geochemical data that can potentially be incorporated into reactive transport modeling experiments.

For the batch reactor experiments, stainless-steel reactors with a 25 mL capacity and Teflon inserts were used. Each reactor was filled with 15 mL of fluid, and 0.1500 g of powdered rock samples (precisely weighed using a four-figure balance) were added, maintaining a rock-to-fluid ratio of 1:100. Subsequently, these reactors

TABLE 1 Elemental composition of geothermal fluids in reservoir wells A and B, as provided by PT Supreme Energy, and the composition of fluids designed for this study. mg/L

Element	Well A	Well B	This study
Na	1020.000	318.000	1000.000
K	188.000	79.800	150.000
Ca	29.400	2.930	20.000
Mg	0.020	<0.010	0
Al	0.326	1.180	0
Cl	1880.000	521.000	1716.000

were sealed. A total of 15 duplicates of this reactor setup were placed in a 100°C oven at the beginning of each experiment. At each time step, one reactor was withdrawn to obtain an individual sample, resulting in a 15-day monitoring period to track the progression of the reaction. The pH of the fluids was measured at room temperature, and the fluids were collected through a 0.22 μm polyethersulfone filter. The solid materials were then dried at 50°C for 2 days. The fluids utilized in each experiment were formulated to mimic the geothermal formation waters found in the RD geothermal well. The composition of these well fluids was provided by PT Supreme Energy, with a partial representation in Table 1. The data suggest that the fluids are meteoric in origin due to their relatively low total dissolved solids and low salinity. The composition of the designed fluids was determined based on an examination of the provided data, with a closer replication of Well A's composition. Solid chloride salts from Fisher Scientific were precisely weighed, with NaCl added to introduce Na^+, KCl for K^+, and $CaCl_2$ for Ca^{2+}, as shown in Table 1. The experiments were conducted with both pH-neutral fluid and acidic fluids adjusted to pH 3 using HCl to simulate the acidic carbon injection conditions seen in other laboratory- and field-scale studies (Alfredsson et al., 2013; Peng et al., 2015) and compare their impact on cation release rates. Additionally, a control experiment with no added rock samples was carried out to assess potential background effects from the experimental setup. The pH and elemental analyses of the fluids in the control experiment were conducted in the same manner as the other experiments.

2.4 | Post-experimental analysis

Post-experimental analysis on the fluid samples was carried out using a Perkin Elmer inductively coupled plasma optical emission spectrometer (ICP-OES). This instrument possesses a detection limit of 0.1 mg/L and offers analytical precision of ≤5%. Calibration standards were created in the range of 0.100–30.000 mg/L using 100.000 mg/L standard solutions from Fisher Chemical for elements Si, Al, Na, K, Ca, and Mg. Each fluid sample was subjected to 1/10 and 1/100 dilutions using 2% HNO_3. The undiluted fluids, as well as the diluted ones, were then analyzed using ICP-OES. Furthermore,

the BET surface area of the solids collected after each experiment was determined using the same method as that applied for the original powdered rock samples before the experiments.

3 | RESULTS

3.1 | Rock characterization

3.1.1 | Microscopy results

The core sample RDB1 hand specimen shows a porphyritic texture, showcasing both dark and pale phenocrysts set within a gray matrix. When observed in
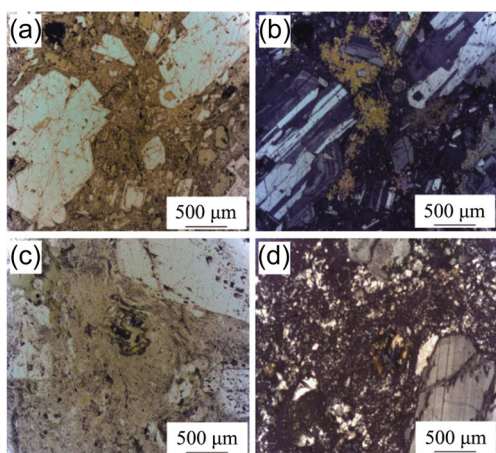

FIGURE 2 Microphotographs of thin sections. (a) Sample RDB1, plane-polarized light. Two substantial feldspar crystals showing that twinning patterns are surrounded by smaller feldspar crystals and a finer-grained matrix. (b) The same view as (a), but observed under crossed-polarized light. (c) Sample RDI1, plane-polarized light. A large feldspar crystal is hosted in a fine-grained matrix, likely composed of quartz and feldspar. (d) The same view as (c), rotated by 90° and observed under crossed-polarized light.

thin section, the larger crystals, measuring up to 5 mm in length, are identified as quartz and feldspars, nestled in a fine-grained matrix (<20 μm) (Figure 2). The presence of a green hue in the matrix surrounding the crystals suggests the occurrence of chlorite, likely formed as a result of hydrothermal alteration.

The core sample RDC1 hand specimen displays an aphanitic and vesicular texture, featuring visible open and sealed fractures, as well as veins, with pronounced gray-green coloring. In thin section, RDC1 reveals veins ranging from 20 to 500 μm in width, filled with various clay minerals and small calcite crystals. Despite the sample's aphanitic texture appearance in the hand specimen, there are larger crystals, reaching up to 3 mm in length, which have been identified as feldspars and quartz, set within a fine-grained matrix. The matrix contains chlorite, evident from its blue-green pleochroism (MacKenzie and Adams, 1994).

The RDI1 hand specimen shows a phaneritic texture, hosting both dark and pale crystals, along with some green coloration, suggesting the presence of chlorite. In thin section, this sample reveals numerous large feldspar crystals, with lengths of up to 2 mm, as well as quartz crystals (Figure 2). Similar to the other samples, a fine-grained matrix embeds the larger crystals.

3.1.2 | Geochemical analysis

The XRF results (Figure 3a) reveal that the composition of sample RDB1 consists of 71% SiO_2, while RDI1 consists of 69% SiO_2. In contrast, RDC1 contains only 53% SiO_2. Furthermore, RDB1 shows higher concentrations of Na_2O and K_2O, but lower concentrations of CaO, MgO, and Fe_2O_3 in comparison with the RDC1 and RDI1 samples.

To investigate the composition of the identified feldspar grains within the thin sections of the samples, microprobe analysis was conducted (Figure 3b). This analysis aimed to
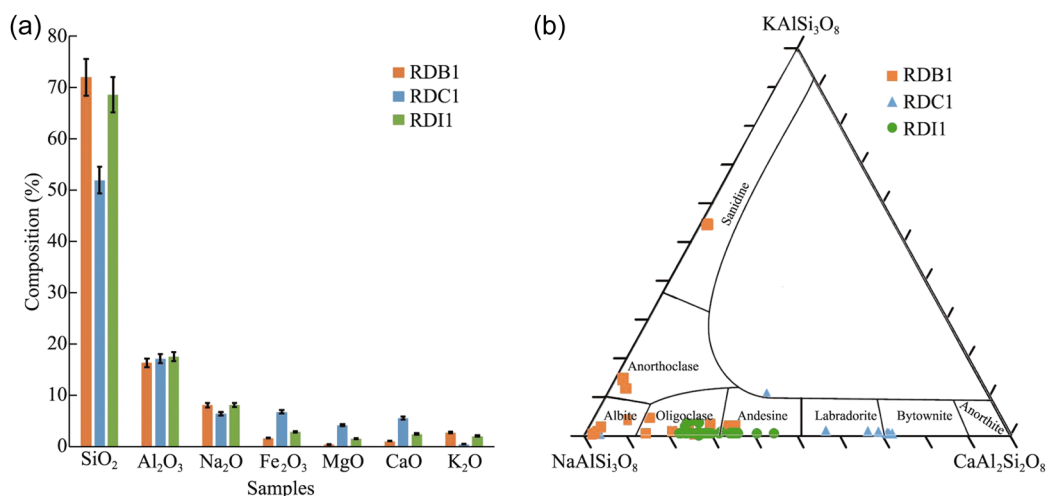

FIGURE 3 Geochemical analysis data. (a) X-ray fluorescence data for the crushed rock samples presented as a percentage of major oxide components, revealing significant differences in the SiO_2 content in the RDC1 sample compared to the other samples (with errors based on a 5% standard machine error). (b) Ternary plot illustrating the compositions of the analyzed feldspar crystals in each sample, as determined through microprobe analysis of the thin sections. This plot indicates that the plagioclase crystals in the RDC1 sample show a more calcic nature compared to the other two samples.

determine the normalized chemical formulas of the feldspar crystals (Table 2) (Deer et al., 2013). Based on 20 analysis points, the feldspar crystals in RDB1 are identified as having an oligoclase–plagioclase composition, with an average formula of $K_{0.04}Na_{0.77}Ca_{0.19}Al_{1.19}Si_{2.81}O_8$. In the case of the RDC1 sample, with data collected from 15 analysis points, the feldspar crystals are determined to have a labradorite–plagioclase composition, with an average formula of $K_{0.02}Na_{0.34}Ca_{0.64}Al_{1.64}Si_{2.36}O_8$. The feldspar crystals in the RDI1 sample, based on 25 analysis points, show an andesine–plagioclase composition, with an average formula of $K_{0.01}Na_{0.68}Ca_{0.31}Al_{1.31}Si_{2.69}O_8$. Importantly, the microprobe data broadly corroborate the findings from the XRF analysis for each sample.

3.1.3 | Mineralogical analysis

The PXRD patterns for the bulk powder samples of RDB1, RDC1, and RDI1 (before clay separation) are depicted in Figure 4, along with the individual patterns for the primary phases present. Semiquantitative PXRD analysis indicates that the RDB1 sample comprises 76% feldspar, 23% quartz, and 1% chlorite. The RDC1 sample consists of 69% feldspar, 21% quartz, and 10% chlorite, while the RDI1 sample is composed of 71% feldspar, 25% quartz, and 4% chlorite. These findings align with the results from microscopy and geochemical characterizations.

In the clay separation experiments ($\leq 2\,\mu m$), it was observed that the RDB1, RDC1, and RDI1 samples contain 5.9%, 13.8%, and 8.7% clay, respectively. Subsequently, these isolated clay fractions were subjected to PXRD analysis, both before and after an acid treatment, confirming the presence of chlorite.

3.2 | Fluid analysis

The results obtained through ICP-OES reveal a time-dependent increase in the Si concentration in all experiments (Figure 5a). Interestingly, under acidic conditions, there is an equivalent or greater release of Si compared to neutral conditions in all samples. Notably, the RDC1 sample in the acidic condition shows the highest Si release, while the RDB1 sample in the neutral condition shows the lowest Si release over the 15-day period. To estimate dissolution rates, a linear fit is applied to the initial Si release, based on the first three data points (Figure 5b), in conjunction with the measured BET surface areas (Table 2), as discussed later. This method of deriving the dissolution rate from the initial data points that follow a linear trend is commonly used in kinetics studies using batch reactor experiments, as the conditions change with time as the reaction proceeds (Peng et al., 2015; Vandeginste et al., 2020, 2021). Once the trend of the data points becomes nonlinear, the system no longer displays a dissolution rate consistent with the starting conditions as it moves toward equilibrium; therefore, only the first three data points were used to estimate the dissolution rates.

Only the RDB1 neutral and RDI1 acidic conditions release a measurable quantity of Al into the fluids, characterized by a rapid increase initially and subsequent stability (Figure 5c). The concentration of Ca in the fluid shows a rapid increase to 5–10 mg/L in all experiments with the RDB1 and RDC1 samples, followed by relative stability. However, in the RDC1 acidic experiment, the concentration continues to increase until the end of the experiment (Figure 5d). In contrast, the RDI1 sample releases a larger quantity of Ca, approximately 40×10^{-6}, at the outset before stabilizing. Generally, the Mg concentration in the fluids is higher under acidic conditions than in neutral conditions for all samples (Figure 5e). Notably, the RDB1 sample in neutral conditions releases negligible Mg, while the RDC1 sample releases the most Mg in the acidic condition. The RDI1 sample, on the other hand, releases similar amounts of Mg under both acidic and neutral conditions. The initial fluids all had 150 mg/L of K added to simulate geothermal fluid conditions, making small changes in its concentration challenging to discern due to increased error margins. The RDI1 sample in both neutral and acidic experiments is the only one that appears to release any K into the fluids (Figure 5f).

In the acidic experiments for all samples, the pH increases rapidly above the initial pH value of 3 (Figure 6). Specifically, the RDB1 sample increases the pH to 6.5, the RDC1 sample to 5.5, and the RDI1 sample to about 7.
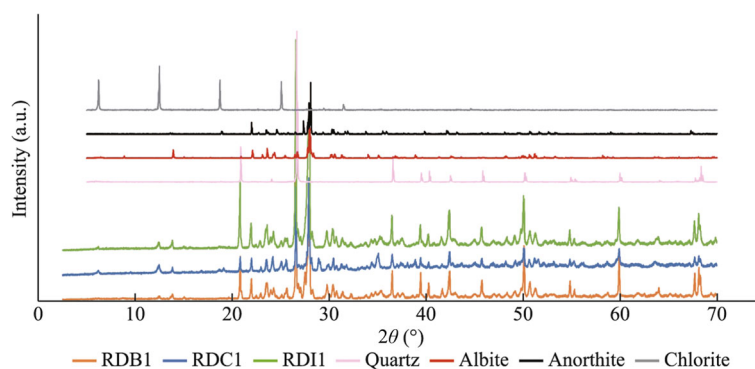

FIGURE 4 Powder X-ray diffraction (PXRD) patterns for the three rock samples, alongside reference PXRD patterns for the identified minerals in the samples, including quartz (Levien et al., 1980), albite (Harlow, 1982), anorthite (Wenk et al., 1980), and chlorite (Phillips et al., 1980). Notably, the most significant differences among the three rock samples are evident in the 5°−20° 2θ region, with more distinct chlorite peaks in the RDC1 sample compared to the other two.
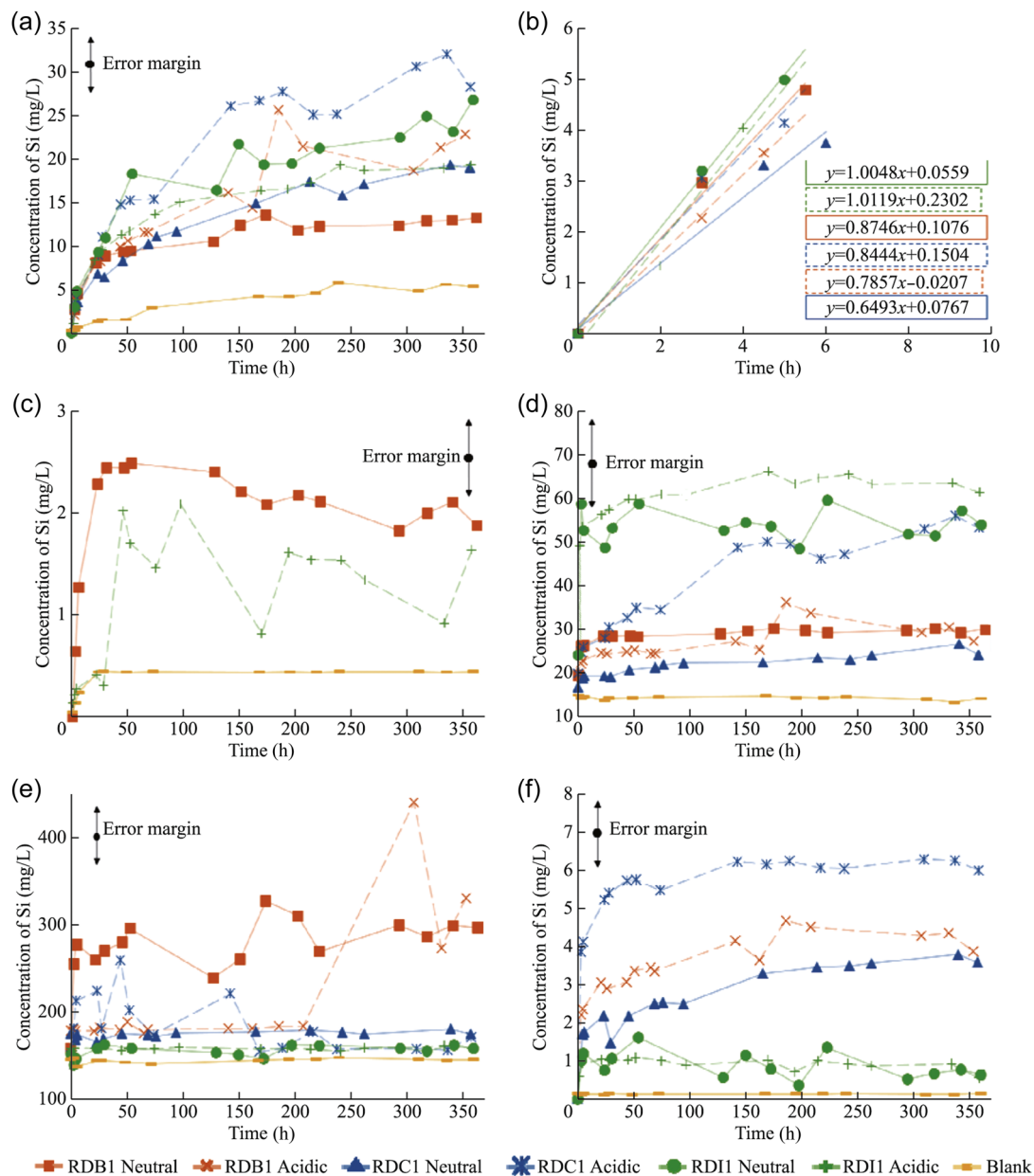
FIGURE 5 Inductively coupled plasma optical emission spectrometer data illustrating elemental concentration changes throughout the experimental periods, measured in mg/L for: (a) silicon release, (b) silicon release within the first 6 h of the experiments, (c) aluminum release, (d) calcium release, (e) potassium release, and (f) magnesium release. Note the varying scales of the vertical axes. Error calculations are based on replicate experiments, resulting in an approximate ±15% margin of error.

The highest pH was recorded in the RDB1 neutral experiment, where the pH reached alkaline levels at 8.5. The fluid pH in the RDC1 sample, both in neutral and acidic experiments, remains below the neutral value of 7, and the fluid pH in the RDI1 sample experiments shows minimal variation between the acidic and neutral conditions.

3.3 | Post-experimental solid analysis

Subsequent to each experiment, PXRD analysis was conducted on the dried solid samples. These patterns displayed slight differences compared to the original samples. However, it is important to note that the solid samples collected at the end of the experiments were dried without disaggregation to prevent minor contamination. As a result, there may be some preferential orientation of the samples on

the XRD holders, which means that these patterns cannot be solely relied upon for precise quantification analysis (Kleeberg et al., 2008). In general, these patterns reveal the same phases as the original samples, but with variations in relative peak heights. Moreover, the surface area of the samples following the fluid–rock reaction was assessed using BET analysis, indicating a minor increase when compared to the original rock sample powder before the experiment (Table 2).

4 | DISCUSSION

4.1 | Mineral dissolution rates

We analyzed the Na–K–Mg ratios based on the fluid data obtained from a geothermal well in Indonesia

TABLE 2 Experimental results including Si release rate [mg/(L·h)] over the first 6 h of the experiment and calculated rock dissolution rate [mol/(m² · s)].

Sample, condition	Average formula	Surface area of rock powder: Initial (final) (m²/g)	Si release rate [mg/(L · h)]	Dissolution rate [10–11 mol/(m² · s)]
RDB1, neutral	$K_{0.04}Na_{0.77}Ca_{0.19}Al_{1.19}Si_{2.81}O_8$	1.1 ± 0.1 (1.0 ± 0.1)	0.8746	4.2
RDB1, acidic	$K_{0.04}Na_{0.77}Ca_{0.19}Al_{1.19}Si_{2.81}O_8$	1.1 ± 0.1 (2.0 ± 0.1)	0.7857	3.8
RDC1, neutral	$K_{0.2}Na_{0.34}Ca_{0.64}Al_{1.64}Si_{2.36}O_8$	1.7 ± 0.1 (3.2 ± 0.1)	0.6493	2.4
RDC1, acidic	$K_{0.2}Na_{0.34}Ca_{0.64}Al_{1.64}Si_{2.36}O_8$	1.7 ± 0.1 (4.7 ± 0.1)	0.8444	3.1
RDI1, neutral	$K_{0.1}Na_{0.68}Ca_{0.31}Al_{1.31}Si_{2.69}O_8$	1.8 ± 0.1 (2.1 ± 0.1)	1.0048	3.1
RDI1, acidic	$K_{0.1}Na_{0.68}Ca_{0.31}Al_{1.31}Si_{2.69}O_8$	1.8 ± 0.1 (2.3 ± 0.1)	1.0119	3.1
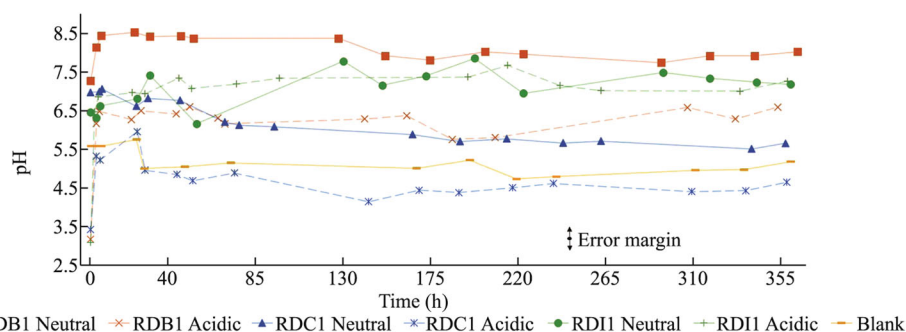
FIGURE 6 Variation in pH measured in the fluids collected over the course of the experiments for each sample and condition. Error is based on the pH meter used, with an accuracy of ±0.1 pH.

(Table 1). We applied Giggenbach's (1988) classification to this data, revealing that the reservoir fluids are not in full equilibrium. Consequently, we expected further mineral dissolution when using simulated geothermal fluids and rock samples (Giggenbach, 1988), which is corroborated by the experimental results. As depicted in Figure 5a, Si is consistently released into the fluids for all samples under the conditions tested. Assessment of the extent of mineral dissolution under neutral and acidic pH conditions provides insights into the magnitude of cation release to be expected when injecting neutral formation waters or those with increased acidity due to dissolved CO_2 for carbon sequestration. It is widely assumed that the rate-limiting step for carbon sequestration through mineral formation [Equation (1)] is the release of divalent cations from mineral dissolution (Oelkers et al., 2008; Wolff-Boenisch et al., 2006). Thus, substantial cation release rates from target rock formations are crucial for successful carbon sequestration. Additionally, the ability of the rock formation to neutralize the acidic pH conditions created by CO_2 dissolution in the fluids is vital for enabling carbonate mineral formation, which necessitates near-neutral or alkaline pH conditions (Matter et al., 2007). Dissolution of minerals like feldspars, known to neutralize solution pH, and the potential release of additional divalent cations can further enhance carbon sequestration (Shibuya et al., 2013). Previous studies have primarily focused on basaltic formations for carbon sequestration via mineral formation (Gislason et al., 2010; Matter et al., 2011; McGrail et al., 2011, 2017; Oelkers et al., 2008) due to their high content of olivine, pyroxene, and plagioclases,

which provide relatively fast divalent cation release. In contrast, our study examines andesite rock samples to assess the potential for carbon sequestration at appreciable levels and within useful time scales, despite significantly lower olivine and pyroxene contents. The mineralogical, geochemical, and microscopic characterization confirms the absence of pyroxene and olivine minerals in all samples investigated in this study.

The investigated rock samples consist mainly of feldspars, quartz, and chlorite. To estimate the dissolution rates of the whole-rock samples, we need to make certain assumptions to simplify the calculation. In this study, we calculate the sample dissolution rates by assuming that the released Si primarily originates from feldspar dissolution (Zhang et al., 2015). Quartz is relatively stable under the experimental conditions in our study, with minimal dissolution rates at pH values between 3 and 7 (Knauss and Wolery, 1988). The dissolution rate of quartz was determined to be approximately 5×10^{-20} mol/(m² · s) by Knauss and Wolery (1988), which is up to 10 orders of magnitude slower than what we would expect for other minerals in the rock samples under these conditions. Therefore, we assume that the dissolution of quartz in this study is negligible and contributes very little to the overall Si release. Chlorite dissolution rates, as indicated by Lowson et al. (2005), are considerably higher, with a rate of 1.78×10^{-13} mol/(m² · s) under neutral pH conditions, and an expected rate of 6.46×10^{-12} mol/(m² · s) under acidic pH conditions. However, given that chlorite constitutes only a relatively small percentage (<10%) of the rock sample and its expected dissolution rate is approximately two orders of magnitude lower than that

for feldspar, we assume that chloride dissolution also contributes very little to the overall Si release.

Considering these assumptions, the release of Si into the fluids is attributed primarily to the dissolution of feldspar in the rock samples. We use a mass balance calculation to determine the sample dissolution rates:

$$R_{\mathrm{dis}} \cdot v_{i,\mathrm{dis}} = \frac{\mathrm{d}C_i}{\mathrm{d}t} \cdot \frac{V}{A_{\mathrm{dis}}}, \tag{2}$$
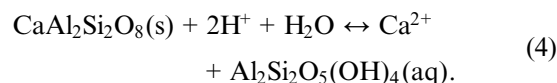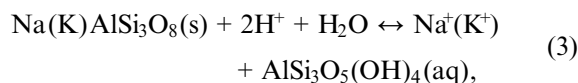
Here, C_i represents the concentration of component i in the reactor, t denotes time, $v_{i,\mathrm{dis}}$ is the stoichiometric coefficient of i in the dissolution reaction, A_{dis} is the surface area of the mineral, V represents the volume of the solution in the reactor, and R_{dis} is the dissolution rate. With a linear change in concentration versus time within the sampling interval, the reaction rate can be calculated by substituting the average change in concentration with time ($\Delta C_i / \Delta t$) for the time derivative of the concentration in Equation (2). To calculate the dissolution rates, we use Si release over the first 6 h of the experiment, as illustrated in Figure 5b, which allows us to approximate far-from-equilibrium conditions in the reactors and simulate the conditions of a hydrothermal system with continuous fluid flow. The average feldspar composition in each sample is determined based on microprobe analysis (Figure 3b). The RDB1 sample has a composition of oligoclase ($K_{0.4}Na_{0.77}Ca_{0.19}Al_{1.19}Si_{2.77}O_8$), with a stoichiometric coefficient of 2.77 for Si used to calculate its dissolution rate. The RDC1 sample is characterized as labradorite ($K_{0.2}Na_{0.34}Ca_{0.64}Al_{1.64}Si_{2.36}O_8$), with a stoichiometric coefficient of 2.36 for Si. The RDI1 sample has a feldspar composition of andesine ($K_{0.1}Na_{0.68}Ca_{0.31}Al_{1.31}Si_{2.68}O_8$), with a stoichiometric coefficient of 2.68 for Si. Previous studies have reported feldspar dissolution rates within a reasonably large range, from 10^{-12} to 10^{-8} mol/(m$^2 \cdot$ s), under similar experimental conditions with pH values between 3 and 4 at 100°C (Carroll and Knauss, 2005; Hellmann, 1994; Oelkers and Schott, 1995; Siegel and Pfannkuch, 1984). The rates calculated in our study fall within this previously reported range (Table 2).

It is worth noting that the dissolution rates calculated from the first 6 h of the experiment do not precisely reflect the final quantity of Si released into the fluids by the end of the experiment. This discrepancy may be attributed to the buffering effects that batch reactor-type experiments often experience. Interestingly, the RDB1 sample in a neutral fluid condition presents the fastest dissolution rate (Table 2), and yet it releases the least Si overall into the fluids by the end of the experiment (Figure 5a). Conversely, the slowest initial dissolution rates are observed for the RDC1 sample in both neutral and acidic pH conditions. Nevertheless, this sample releases a relatively high amount of Si by the end of the experiment, especially in the acidic condition, resulting in higher overall Si release throughout the entire experiment. Semiquantitative PXRD results indicate that the RDB1 sample, which shows the fastest initial dissolution rate, corresponds to the sample with the highest feldspar content. In contrast, the RDC1 sample, with the slowest initial dissolution rate, has the lowest feldspar

content. Microprobe results further indicate that the RDC1 sample contains feldspars with a higher calcium content, while the RDB1 sample contains feldspars with a higher sodium content. Previous studies have shown that calcic feldspars are less stable under acidic conditions compared to alkali feldspars. This may explain why the RDC1 sample releases more Si overall, with the controlling factors of feldspar content, feldspar dissolution rate, and changing pH affecting the fluid–rock interaction in the batch reactors (Blum, 2012; Casey et al., 1991; Oelkers and Schott, 1995). Likewise, geochemical modeling of CO$_2$ injection in host rocks in the Ungaran geothermal field indicates that anorthite (calcium feldspar) dissolution dominates over the dissolution of other minerals and that calcite precipitates at the expense of anorthite dissolution (Utomo and Güleç, 2021). Therefore, our findings suggest that the dissolution rates derived from the first 6 h of the experiment were more influenced by the feldspar content in the rock sample, with a faster rate of Si release for sample RDB1, which has the highest feldspar content. However, the overall magnitude of mineral dissolution after a 15-day period was influenced more by the type of feldspar mineral in the rock sample. RDC1, which contains less stable calcic-type plagioclase, released more Si by the end of the experimental duration compared to RDB1, which has sodic-type plagioclase. In the RDC1 experiment under acidic conditions, the pH remained lower for a longer time in the batch reactors, thus favoring higher dissolution rates.

4.2 | pH buffering capacity

The initial rapid pH buffering observed in Figure 5 can be explained by feldspar dissolution, which consumes H$^+$ ions. This process is depicted in Equation (3) for alkali feldspars and Equation (4) for calcic feldspars (Matter et al., 2011; Shibuya et al., 2013; Zhang et al., 2015):

$$\mathrm{Na(K)AlSi_3O_8(s)} + 2\mathrm{H}^+ + \mathrm{H_2O} \leftrightarrow \mathrm{Na}^+(\mathrm{K}^+) \\ + \mathrm{AlSi_3O_5(OH)_4(aq)}, \tag{3}$$

$$\mathrm{CaAl_2Si_2O_8(s)} + 2\mathrm{H}^+ + \mathrm{H_2O} \leftrightarrow \mathrm{Ca}^{2+} \\ + \mathrm{Al_2Si_2O_5(OH)_4(aq)}. \tag{4}$$

In the experiments conducted with the RDB1 and RDI1 samples, the solution pH increases more significantly than in the experiment involving the RDC1 sample (Figure 6). Given that the RDC1 sample has the lowest feldspar content, it is likely that the availability of feldspar for dissolution is limited, resulting in less effective buffering of the acidic pH solutions over the 15-day time scale in this study. In the context of carbon sequestration, it is crucial for H$^+$ ions causing acidity in the fluids to be consumed through reactions such as feldspar dissolution. This consumption allows the fluids to reach neutral pH levels suitable for carbonate precipitation (Gislason et al., 2010). Consequently, the findings of this study suggest that rock systems with high

feldspar content are promising candidates for carbon sequestration via carbonate mineral formation. The fluid pH can be adequately buffered, depending on factors such as fluid-rock ratio, fluid composition, temperature, and fluid flow conditions.

4.3 | Secondary mineral formation

Despite the presence of Al in feldspar in the samples and ongoing feldspar dissolution, detectable Al concentrations are only found in the fluids from experiments with RDB1 under neutral conditions and RDI1 under acidic conditions. Based on the measured feldspar composition (between oligoclase and labradorite), Al release in the fluids would be expected at levels about two to three times lower than that of Si. However, in some experiments, up to 30×10^{-6} of Si is released without any detectable Al release. This implies that significant nonstoichiometric dissolution must be occurring, or there is secondary mineral formation removing Al from the solution.

In the different experiments, the pH increased most significantly, reaching approximately 8.5, over the course of the experiment for the RDB1 sample under neutral conditions. Previous research conducted under similar experimental conditions showed the formation of aluminum hydroxide precipitates at a pH of 5–9 (Balintova and Petrilakova, 2011). Gibbsite (Al(OH)$_3$) precipitates preferentially in an acidic environment, and the bayerite polymorph forms readily in a solution with a pH above 5.8 (Barnhisel and Rich, 1965; Schoen and Roberson, 1970). Therefore, the lack of detectable Al in most experiments may be due to the rapid precipitation of aluminum hydroxide species in solutions with a pH between 5 and 7. The higher pH values in the RDB1 neutral experiment, particularly within the first few hours, could inhibit some aluminum hydroxide precipitation due to less favorable alkaline conditions, leading to a small detectable Al concentration in the fluids (Figure 5c). These observations have implications for the availability of divalent cations for carbonate formation, as any secondary precipitates may capture some divalent cations (such as Fe^{2+}) in their structures, reducing the cations available for carbonate mineral formation (Gysi and Stefánsson, 2011). Therefore, additional research may be needed to assess the potential impact of aluminum hydroxide precipitation on the implementation of carbon sequestration in geothermal reservoirs at a field scale.

Moreover, other research involving reactive transport calculations has highlighted the importance of secondary mineral formation kinetics in CO$_2$ mineralization for subsurface storage (Addassi et al., 2024). In the study, it was calculated that carbonation of fresh basaltic glass was slower initially, taking account of the lower secondary silicate mineral (clay and zeolite) precipitation rates. It was explained in the study that the calculated higher aluminum ion concentration in the fluids caused slower dissolution rates of primary basaltic glass. In contrast, the carbonation rate of hydrothermally altered basalts was found to be faster when taking account of slow secondary silicate mineral precipitation.

4.4 | Implications for carbon storage in andesitic reservoirs

Studies at the field scale involving carbon sequestration in basaltic reservoirs have reported impressive results, with up to 95% of injected CO$_2$ mineralized in under 2 years (Matter et al., 2016). This method of carbon trapping through mineralization offers a significant advantage compared to other approaches like structural trapping, which relies on impermeable cap rocks to prevent CO$_2$ leakage. Basalt shows dissolution rates on the order of 10^{-10} mol/(m$^2 \cdot$ s) (Gudbrandsson et al., 2011), whereas the dissolution rate of andesite, as determined in our study, has a magnitude of about 10^{-11} mol/(m$^2 \cdot$ s) The faster dissolution of basalt can be attributed to its distinct mineralogy, featuring minerals like olivine with an average dissolution rate of 10^{-8} mol/(m$^2 \cdot$ s) (Rimstidt et al., 2012). Faster dissolution of rock is beneficial because it makes more divalent cations available in a shorter time frame, offering the potential for faster CO$_2$ trapping through mineralization. The andesite dissolution rate observed in our study, which is roughly one to two orders of magnitude lower than that of basalt, aligns well with rates reported in previous studies on volcanic glasses with higher silica content under acidic and more ambient temperature conditions (Wolff-Boenisch et al., 2004, 2006). Previous research suggests that, in cases where a volcanic glass sample with high silica content shows dissolution rates approximately two orders of magnitude slower than one with lower silica content, Ca release rates follow a similar trend (Wolff-Boenisch et al., 2006). Therefore, we assume that a comparable trend applies to the crystalline rock samples used in our present study. Although the release rate of calcium divalent cations is slower in andesite samples compared to basalt samples, andesitic reservoirs are still likely to be suitable for carbon sequestration. However, it is expected to take longer for the fluids to reach a state of carbonate mineral saturation. This will generally lead to slower carbonate mineral formation, but these minerals are also likely to precipitate further away from the injection site in andesite reservoirs as compared to basalt reservoirs. This could be beneficial in preventing the potential risks of permeability reduction associated with mineral precipitation close to the injection site. Other forms of geological carbon storage, like injection into porous sedimentary-type reservoirs that rely on solution trapping (Holloway, 1997), can take more than 1000 years to serve as permanent, secure storage sites for CO$_2$. In contrast, results from field-scale studies on mineral trapping in basaltic reservoir rocks have shown the potential for permanent storage in 2 years or less (Matter et al., 2016; McGrail et al., 2017; Pogge von Strandmann et al., 2019; Snæbjörnsdóttir et al., 2020). Also, in altered basaltic rocks, reaction path calculations suggest that 95% of injected water-dissolved CO$_2$ would be trapped in minerals within 5 years at 100°C (Oelkers et al., 2022). Even though andesitic reservoirs may have slightly slower trapping rates compared to basaltic reservoirs, they are still likely to achieve permanent CO$_2$ storage at a significantly faster rate than what is achievable with solubility trapping in porous sedimentary-type reservoirs. These findings align with geochemical modeling results of CO$_2$ injection in the Ungaran geothermal field, which predict the dissolution of

calcic feldspar coupled with calcite precipitation as a CO_2 mineralization mechanism and a progressive transition from solubility to mineral trapping within 30 days upon injection (Utomo and Güleç, 2021).

Divalent species like Mg^{2+} and Fe^{2+} are also essential considerations when discussing carbon sequestration through mineral trapping. These species are abundant in basaltic rock types, which is why they have been a focal point in previous studies on these rocks and one of the key reasons why basaltic rocks are seen as the optimal target for rapid mineral trapping of CO_2 (Matter et al., 2016; Snæb-jörnsdóttir et al., 2020). In contrast, these species are considerably less abundant in andesite-type rocks because plagioclase minerals do not contain Mg or Fe as major elements. In the current study, minor amounts of Mg^{2+} were detected in the fluids, particularly in experiments using the RDC1 sample (Figure 5e). The latter sample had the highest (although still relatively low) chlorite content. Mg is often present within the chlorite structure, so the release of Mg may be due to the minor dissolution of this mineral. The XRF geochemical analysis of the samples supports this interpretation, indicating that sample RDC1 has a higher MgO content compared to the other samples (Figure 3a). While our study has focused on the release of Ca from plagioclase minerals within andesitic rocks, the significance of Mg release from other samples with higher secondary mineral content is an area of research that could be further explored, with relevance to divalent cation release for carbon sequestration.

Our study presents promising results for potential carbon storage through carbonate mineral formation in andesitic reservoirs, indicating the need for further investigation and field trials. Apart from Indonesia, regions like New Zealand are highlighted for their andesite rock resources and geothermal energy exploration. To initiate a demonstration pilot project in andesitic reservoirs, further comprehensive studies that consider additional factors are required. These factors include assessing the permeability of target reservoirs, ensuring sufficient pore space for carbonate mineral formation, evaluating the importance of a sufficiently low-permeability "cap-rock" to prevent CO_2 leakage, and conducting additional laboratory experiments under different temperature conditions relevant to various target formations worldwide. We have found that the specific rock mineralogy plays a pivotal role in predicting the suitability of andesitic reservoirs for carbon sequestration. Rocks with a high content of calcium-rich plagioclase are favored, especially if minerals such as olivine and pyroxene, found in basalt, are not available. The results of this study contribute to the knowledge required for the initial assessment of the feasibility of sequestering CO_2 in andesitic rock systems, which can be a significant contribution to global greenhouse gas mitigation efforts.

5 | CONCLUSIONS

The study yields several key findings:

1. The dissolution of rock samples released a greater quantity of divalent cations when the calcic plagioclase content was higher. This suggests that formations rich in calcic plagioclase may be preferable targets, especially when olivine and pyroxene minerals are absent, as they release the necessary divalent cations essential for carbonate mineral formation.

2. Samples with a higher overall plagioclase mineral content demonstrated more effective buffering capacity in experiments under acidic conditions. Andesite reservoirs with a substantial plagioclase content are likely to be well-suited for carbon sequestration. They can help transform the initially acidic pH fluids, saturated with dissolved CO_2, into near-neutral pH conditions suitable for carbonate mineral formation.

3. The lower-than-expected concentrations of Al in the fluids indicate that secondary mineral formation is likely occurring, affecting cation removal from solutions. Further research is warranted to assess the impact of such secondary mineral formation.

4. The andesite rock samples used in this study showed dissolution rates approximately one to two orders of magnitude slower than those reported for basalt rock samples. While this may imply that carbon sequestration in andesitic reservoirs is comparatively slower than that in basaltic reservoirs, it is essential to note that carbonate mineral formation in andesitic reservoirs remains a highly viable option due to its relative rapidity.

In summary, the outcomes of this study underscore the importance of further exploration of carbon sequestration via carbonate mineral formation in andesitic rock formations. Although basaltic rock types are likely to yield optimum conditions for carbon sequestration via mineralization, this approach suggests that andesitic reservoirs may be a suitable alternative for carbon sequestration when basaltic rock types are unavailable. Further research incorporating geochemical data relating to these andesitic rock types into reactive transport simulations, alongside appropriate core flooding-type experiments, would provide further valuable insights for the field. Our study contributes valuable insights into the feasibility of sequestering CO_2 in andesitic rock systems, offering a means to mitigate the ongoing global release of greenhouse gases, which continues to accelerate global warming and climate change.

CONFLICT OF INTEREST STATEMENT

The authors declare no conflict of interest.

DATA AVAILABILITY STATEMENT

The data that support the findings of this study are available from the corresponding author upon reasonable request.

ORCID

Veerle Vandeginste http://orcid.org/0000-0003-0950-7089

REFERENCES

Addassi M, Hoteit H, Oelkers EH. The impact of secondary silicate mineral precipitation kinetics on CO_2 mineral storage. *Int J Greenhouse Gas Control*. 2024;131:104020.

Alfredsson HA, Oelkers EH, Hardarsson BS, Franzson H, Gunnlaugsson E, Gislason SR. The geology and water chemistry of the Hellisheidi, SW-Iceland carbon storage site. *Int J Greenhouse Gas Control*. 2013;12:399-418. doi:10.1016/j.ijggc.2012.11.019

Aradóttir ESP, Gunnarsson I, Sigfússon B, et al. Toward cleaner geothermal energy utilization: capturing and sequestering CO_2 and H_2S emissions from geothermal power plants. *Transport Porous Med*. 2015;108:61-84. doi:10.1007/s11242-014-0316-5

Balintova M, Petrilakova A. Study of pH influence on selective precipitation of heavy metals from acid mine drainage. In: Klemes J, Varbanov PS, Lam HL, eds. *14th International Conference on Progress Integration, Modelling and Optimisation for Energy*. Vol. 25. 2011:10.

Barber AJ, Crow MJ, Milsom JS. *Sumatra: Geology, Resources and Tectonic Evolution*. The Geological Society; 2005.

Barnhisel RI, Rich CI. Gibbsite, bayerite, and nordstrandite formation as affected by anions, pH, and mineral surfaces. *Soil Sci Soc Am J*. 1965;29:531-534.

Biscaye PE. Distinction between kaolinite and chlorite in recent sediments by X-ray diffraction. *Am Mineral*. 1964;49:1281-1289.

Blum AE. Feldspars in weathering. In: Parsons I, ed. *Feldspars and Their Reactions*. Springer; 2012:595-609. doi:10.1007/978-94-011-1106-5

Boedihardi M, Mulyonol A, Ginting A, Mosby M, Radja V. Geology, energy potential and development of Indonesia's geothermal prospects. *Geological Society of Malaysia-Circum-Pacific Council for Energy and Mineral Resources Tectonic Framework and Energy Resources of the Western Margin of the Pacific Basin November 27-December 2, 1992, Kuala Lumpur, Malaysia*. 1993;33:369-385.

Carroll SA, Knauss KG. Dependence of labradorite dissolution kinetics on CO_2(aq), Al(aq), and temperature. *Chem Geol*. 2005;217:213-225. doi:10.1016/j.chemgeo.2004.12.008

Casey WH, Westrich HR, Holdren GR. Dissolution rates of plagioclase at pH = 2 and 3. *Am Mineral*. 1991;76:211-217.

Clark DE, Galeczka IM, Dideriksen K, Voigt MJ, Wolff-Boenisch D, Gislason SR. Experimental observations of CO_2-water-basaltic glass interaction in a large column reactor experiment at 50°C. *Int J Greenhouse Gas Control*. 2019;89:9-19. doi:10.1016/j.ijggc.2019.07.007

Clark DE, Oelkers EH, Gunnarsson I, et al. CarbFix2: CO_2 and H_2S mineralization during 3.5 years of continuous injection into basaltic rocks at more than 250°C. *Geochim Cosmochim Acta*. 2020;279:45-66.

Deer WA, Howie RA, Zussman J. *An Introduction to the Rock-Forming Minerals*. 3rd ed. Mineralogical Society of Great Britain and Ireland; 2013. doi:10.1180/DHZ

Department of Energy and Climate Change. UK Energy Statistics, 2015 and Q4 2015. Statistical Press Release; 2016:116.

Edenhofer O, Pichs-Madruga R, Sokona Y, et al. *Climate change 2014: Mitigation of Climate Change. Contribution of Working Group III to the Fifth Assessment Report of the Intergovernmental Panel on Climate Change, IPCC*. Cambridge University Press; 2014.

Erol S, Akin T, Akin S. Update for reactive transport modeling of the Kızıldere geothermal field to reduce uncertainties in the early inspections. *Turk J Earth Sci*. 2023;32(4):541-554.

Fridriksson T, Mateos-Merino A, Audinet P, Orucu AY. Greenhouse gases from geothermal power production. *Proceedings, 42nd Workshop on Geothermal Reservoir Engineering Stanford University, Stanford, California, February 13-15, 2017, SGP-TR-212*, 2016:1-12.

Galeczka IM, Stefánsson A, Kleine BI, et al. A pre-injection assessment of CO_2 and H_2S mineralization reactions at the Nesjavellir (Iceland) geothermal storage site. *Int J Greenhouse Gas Control*. 2022;115:103610.

Giggenbach WF. Geothermal solute equilibria. Derivation of Na-K-Mg-Ca geoindicators. *Geochim Cosmochim Acta*. 1988;52:2749-2765. doi:10.1016/0016-7037(88)90143-3

Gíslason SR, Sigurdardóttir H, Aradóttir ES, Oelkers EH. A brief history of CarbFix: challenges and victories of the project's pilot phase. *Energy Procedia*. 2018;146:103-114. doi:10.1016/j.egypro.2018.07.014

Gislason SR, Wolff-Boenisch D, Stefansson A, et al. Mineral sequestration of carbon dioxide in basalt: a pre-injection overview of the CarbFix project. *Int J Greenhouse Gas Control*. 2010;4:537-545. doi:10.1016/j.ijggc.2009.11.013

Gudbrandsson S, Wolff-Boenisch D, Gislason SR, Oelkers EH. An experimental study of crystalline basalt dissolution from $2 \leq pH \leq 11$ and temperatures from 5 to 75°C. *Geochim Cosmochim Acta*. 2011;75:5496-5509. doi:10.1016/j.gca.2011.06.035

Gysi AP, Stefánsson A. CO_2–water–basalt interaction. Numerical simulation of low temperature CO_2 sequestration into basalts. *Geochim Cosmochim Acta*. 2011;75:4728-4751. doi:10.1016/j.gca.2011.05.037

Hangx SJT, Spiers CJ. Reaction of plagioclase feldspars with CO_2 under hydrothermal conditions. *Chem Geol*. 2009;265:88-98. doi:10.1016/j.chemgeo.2008.12.005

Harlow GE. The anorthoclase structures: the effects of temperature and composition. *Am Mineral*. 1982;67:975-996.

Hellmann R. The albite-water system: part I. The kinetics of dissolution as a function of pH at 100, 200, and 300°C. *Geochim Cosmochim Acta*. 1994;58:595-611. doi:10.1016/0016-7037(94)90491-X

Holloway S. An overview of the underground disposal of carbon dioxide. *Energy Convers Manage*. 1997;38:S193-S198. doi:10.1016/s0196-8904(96)00268-3

Intergovernmental Panel on Climate Change (IPCC). Summary for policymakers. In: Masson-Delmotte V, Zhai P, Portner H-O, et al. eds. *Global Warming of 1.5°C*. IPCC; 2018.

International Centre for Diffraction Data (ICDD). *PDF-4*, 2018.

Kleeberg R, Monecke T, Hillier S. Preferred orientation of mineral grains in sample mounts for quantitative XRD measurements: how random are powder samples? *Clays Clay Miner*. 2008;56:404-415. doi:10.1346//CCMN.2008.0560402

Knauss KG, Wolery TJ. The dissolution kinetics of quartz as a function of pH and time at 70°C. *Geochim Cosmochim Acta*. 1988;52:43-53. doi:10.1016/0016-7037(88)90055-5

Levien L, Prewitt CT, Weidner DJ. Structure and elastic properties of quartz at pressure. *Am Mineral*. 1980;65:920-930.

Lo Ré C, Kaszuba JP, Moore JN, McPherson BJ. Fluid–rock interactions in CO_2-saturated, granite-hosted geothermal systems: implications for natural and engineered systems from geochemical experiments and models. *Geochim Cosmochim Acta*. 2014;141:160-178.

Lowson RT, Comarmond M-CJ, Rajaratnam G, Brown PL. The kinetics of the dissolution of chlorite as a function of pH and at 25°C. *Geochim Cosmochim Acta*. 2005;69:1687-1699. doi:10.1016/j.gca.2004.09.028

MacKenzie WS, Adams AE. *A Colour Atlas of Rocks and Minerals in Thin Section*. 2nd ed. Manson Publishing Ltd; 1994.

Matter JM, Broecker WS, Gislason SR, et al. The CarbFix pilot project—storing carbon dioxide in basalt. *Energy Procedia*. 2011;4:5579-5585. doi:10.1016/j.egypro.2011.02.546

Matter JM, Stute M, Snæbjörnsdottir SÓ, et al. Rapid carbon mineralization for permanent disposal of anthropogenic carbon dioxide emissions. *Science*. 2016;352:1312-1314. doi:10.1126/science.aad8132

Matter JM, Takahashi T, Goldberg D. Experimental evaluation of in situ CO_2 water rock reactions during CO_2 injection in basaltic rocks: implications for geological CO_2 sequestration. *Geochem Geophys Geosystems*. 2007;8:Q02001. doi:10.1029/2006GC001427

McCarthy JJ, Canziani OF, Leary NA, Dokken D, White KS. *Climate Change 2001: Impacts, Adaptation, and Vulnerability*. Cambridge University Press; 2001.

McGrail BP, Schaef HT, Ho AM, Chien Y-J, Dooley JJ, Davidson CL. Potential for carbon dioxide sequestration in flood basalts. *J Geophys Res Solid Earth*. 2006;111:B12201. doi:10.1029/2005JB004169

McGrail BP, Schaef HT, Spane FA, et al. Wallula basalt pilot demonstration project: post-injection results and conclusions. *Energy Procedia*. 2017;114:5783-5790. doi:10.1016/j.egypro.2017.03.1716

McGrail BP, Spane FA, Sullivan EC, Bacon DH, Hund G. The Wallula basalt sequestration pilot project. *Energy Procedia*. 2011;4:5653-5660. doi:10.1016/j.egypro.2011.02.557

Muraoka H, Takahashi M, Sundhoro H, et al. Geothermal systems constrained by the Sumatran fault and its pull-apart basins in Sumatra, Western Indonesia. *Proceedings World Geothermal Congress 2010Bali, Indonesia, 2-29 April 2010 GV Tomarov and AA Shipkov*. Vol. 57. 2010.

Na J, Xu T, Yuan Y, Feng B, Tian H, Bao X. An integrated study of fluid–rock interaction in a CO_2-based enhanced geothermal system: a case study of Songliao basin, China. *Appl Geochem*. 2015;59:166-177.

Oelkers EH, Arkadakskiy S, Afifi AM, et al. The subsurface carbonation potential of basaltic rocks from the Jizan region of southwest Saudi Arabia. *Int J Greenhouse Gas Control*. 2022;120:103772.

Oelkers EH, Gislason SR, Matter J. Mineral carbonation of CO_2. *Elements*. 2008;4:333-337. doi:10.2113/gselements.4.5.333

Oelkers EH, Schott J. Experimental study of anorthite dissolution and the relative mechanism of feldspar hydrolysis. *Geochim Cosmochim Acta*. 1995;59:5039-5053. doi:10.1016/0016-7037(95)00326-6

Peng C, Crawshaw JP, Maitland GC, Trusler JPM. Kinetics of calcite dissolution in CO_2-saturated water at temperatures between 323 and 373 K and pressures up to 13.8 MPa. *Chem Geol*. 2015;403:74-85.

Phillips TL, Loveless JK, Bailey SW. Cr3+ coordination in chlorites: a structural study of ten chromian chlorites. *Am Mineral*. 1980;65:112-122.

Pogge von Strandmann PAE, Burton KW, Snæbjörnsdóttir SO, et al. Rapid CO_2 mineralisation into calcite at the CarbFix storage site quantified using calcium isotopes. *Nat Commun*. 2019;10:1983. doi:10.1038/s41467-019-10003-8

Purnomo BJ, Pichler T. Geothermal systems on the island of Java, Indonesia. *J Volcanol Geotherm Res*. 2014;285:47-59. doi:10.1016/j.jvolgeores.2014.08.004

Ratouis TMP, Snæbjörnsdóttir SÓ, Voigt MJ, et al. CarbFix 2: a transport model of long-term CO_2 and H_2S injection into basaltic rocks at Hellisheidi, SW-Iceland. *Int J Greenhouse Gas Control*. 2022;114:103586.

Rimstidt JD, Brantley SL, Olsen AA. Systematic review of forsterite dissolution rate data. *Geochim Cosmochim Acta*. 2012;99:159-178. doi:10.1016/j.gca.2012.09.019

Santoso D, Suparka ME, Sudarman S, Sauri S. The geothermal fields in central part of the Sumatra fault zone as derived from geophysical data. In: Barbier E, ed. *Proceedings of the Wolrd Geothermal Congress*. International Geothermal Association; 1995:1363-1366.

Sawin J, Seyboth K, Sverrisson F. *Renewables 2017 Global Status Report*. REN21: Renewable Energy Policy Network for the 21st Century; 2017.

Schoen R, Roberson CE. Structures of aluminum hydroxide and geochemical implications. *Am Mineral*. 1970;55:43-77.

Shibuya T, Yoshizaki M, Masaki Y, Suzuki K, Takai K, Russell MJ. Reactions between basalt and CO_2-rich seawater at 250 and 350°C, 500bars: implications for the CO_2 sequestration into the modern oceanic crust and the composition of hydrothermal vent fluid in the CO_2-rich early ocean. *Chem Geol*. 2013;359:1-9. doi:10.1016/j.chemgeo.2013.08.044

Siegel DI, Pfannkuch HO. Silicate mineral dissolution at pH 4 and near standard temperature and pressure. *Geochim Cosmochim Acta*. 1984;48:197-201. doi:10.1016/0016-7037(84)90362-4

Sieh K, Natawidjaja D. Neotectonics of the Sumatran fault, Indonesia. *J Geophys Res Solid Earth*. 2000;105:28295-28326. doi:10.1029/2000JB900120

Snæbjörnsdóttir SÓ, Sigfússon B, Marieni C, Goldberg D, Gislason SR, Oelkers EH. Carbon dioxide storage through mineral carbonation. *Nat Rev Earth Environ*. 2020;1:90-102. doi:10.1038/s43017-019-0011-8

Suharmanto P, Fitria AN, Ghaliyah S. Indonesian geothermal energy potential as source of alternative energy power plant. *Renewable Energy and Energy Conversion Conference and Exhibition*. Knowledge E; 2015:119-124. doi:10.18502/ken.v1i1.325

Utomo GP, Güleç N. Preliminary geochemical investigation of a possible CO_2 injection in the Ungaran geothermal field, Indonesia: equilibrium and kinetic modeling. *Greenhouse Gases Sci Technol*. 2021;11(1):3-18.

Vandeginste V, Cowan C, Gomes RL, Hassan T, Titman J. Natural fluorapatite dissolution kinetics and Mn^{2+} and Cr^{3+} metal removal from sulfate fluids at 35°C. *J Hazard Mater*. 2020;389:122150.

Vandeginste V, Siska A, Belshaw G, Kilpatrick A. Effect of salinity on the kinetics of pyrite dissolution in oxygenated fluids at 60°C and implications for hydraulic fracturing. *J Nat Gas Sci Eng*. 2021;86:103722.

Wenk H-R, Joswig W, Tagai T, Korekawa M, Smith BK. The average structure of An 62-66 labradorite. *Am Mineral*. 1980;65:81-95.

Wolff-Boenisch D, Gislason SR, Oelkers EH. The effect of crystallinity on dissolution rates and CO_2 consumption capacity of silicates. *Geochim Cosmochim Acta*. 2006;70:858-870. doi:10.1016/j.gca.2005.10.016

Wolff-Boenisch D, Gislason SR, Oelkers EH, Putnis CV. The dissolution rates of natural glasses as a function of their composition at pH 4 and 10.6, and temperatures from 25 to 74°C. *Geochim Cosmochim Acta*. 2004;68:4843-4858. doi:10.1016/j.gca.2004.05.027

Wu Y, Li P, Hao Y, Wanniarachchi A, Zhang Y, Peng S. Experimental research on carbon storage in a CO_2-based enhanced geothermal system. *Renew Energy*. 2021;175:68-79.

Zhang R, Zhang X, Hu S. Basalt-water interactions at high temperatures: 1. Dissolution kinetic experiments of basalt in water and $NaCl-H_2O$ at temperatures up to 400°C, 23MPa and implications. *J Asian Earth Sci*. 2015;110:189-200. doi:10.1016/j.jseaes.2015.03.042

AUTHOR BIOGRAPHY

Veerle Vandeginste is an associate professor in the Department of Materials Engineering at KU Leuven, Belgium, since 2020. She obtained a PhD in Geology at KU Leuven in 2006. Following research positions at the Geological Survey of Belgium and then at Cerege (Aix-en-Provence, France), she was a research fellow at the Department of Earth Science and Engineering at Imperial College London, United Kingdom. In 2015, she was appointed as an assistant professor at the University of Nottingham, where she established the geochemistry research discipline in the School of Chemistry, and was promoted to associate professor in 2020. She received several institutional and international awards, such as the Arthur Holmes Centenary Research Award, the Stephen E. Laubach Research in Structural Diagenesis Award, and GDL

Foundation Research Fellowship. Currently, she conducts research on materials for sustainable solutions, focusing on the study and optimization of physical and chemical properties of the contact and interaction between materials, for energy storage, conversion and efficiency, gas storage and conversion, and healthcare devices.